CHAPTER - 2

EXPERIMENTAL DETAILS

Chapter – 2

EXPERIMENTAL DETAILS

This chapter provides background information on materials selection, synthesis and characterization techniques employed for carrying out the investigations illustrated in third, fourth and fifth chapters. Aluminum based crystalline, composite alloys and intermetallic compounds are of special interest in the present experimental work. Non-equilibrium materials processing technique notably mechanical alloying/milling via high-energy ball milling have been extensively employed for the current work and are discussed in detail. The effect of milling time, extent of alloying, role of alloying elements, dispersion of reinforcement on the structure, morphology and mechanical properties of composite powders are investigated. In case of intermetallic compounds the MM powder samples were characterized for determining the sequence of structural evolution involving formation of amorphous and/or nanocrystalline or any other metastable phases and their stability in the systems studied.

2.1 Materials selection and processing

In the present investigation mechanical alloying (MA) was carried to produce Al-based composite alloys and mechanical milling for intermetallic powders of pre-alloyed ingots. Gas atomized powders of aluminum alloy, grade EN AW6082 with 99% purity, having particle size < 75 μm (supplied by Kemphasol Ltd., India) and aluminum powder of 99.7% purity (Merck, Germany) were used as a matrix material. Beach sand garnet powder of 99.5% purity with a particulate size range of 50-100 μm

(supplied by Indian Rare Earths Limited, Manavalakurichi, India) and multi-walled carbon nanotubes (MWCNTs) produced by chemical vapor deposition (CVD) having a purity of 95% and an average diameter and length of 20 nm and 5 μm, respectively, (supplied by Nanoshel) were used as reinforcement. The fraction of the garnet and CNTs used as reinforcement in the EN AW6082 alloy was kept at 5 wt.% and 2 wt.%. The chemical composition of EN AW6082 Al-alloy powder and average chemical composition of reinforcement garnet

Table 2.1: Chemical composition of the matrix – gas atomized Aluminum alloy powder EN AW6082.

Element's concentration (wt. %)							
Si	Mg	Mn	Fe	Cr	Cu	Zn	Al
1.2	0.78	0.50	0.33	0.14	0.08	0.05	Bal.

Table 2.2: Chemical composition of the reinforcement particle – Garnet.

Constituent (oxides), wt. %						
SiO_2	Al_2O_3	TiO_2	Fe_2O_3	CaO	MgO	MnO
36.15	19.09	0.57	32.87	3.41	7.22	0.69

particles are given (Table 2.1 and 2.2). In case of intermetallics, alloys of nominal composition of Al-25 at.%Fe, Al-30 at.Fe%, Al-34.5 at.%Fe, Al-50 at.%Fe and Al-75 at.%Fe close to Al_3Fe, Al_5Fe_2, Al_2Fe, FeAl and Fe_3Al intermetallic phases were prepared using pure constituent elements (Al-99.9 wt.%, Fe-99.96 wt.%) in an arc

melting furnace with a water cooled copper hearth, under argon atmosphere. To overcome the inevitable mass loss of these reactants, a slight excess (usually 0.5 - 1.0 wt. %) of the particular element is loaded. The ingots were re-melted 3-5 times to ensure chemical homogeneity. Further, the as-cast alloys obtained were homogenized at 1000^{o}C for 2 hour. Al rich pre-alloyed ingots were brittle and were mechanically crushed to powders of less than 10 μm size, whereas ingots with 25 and 50 % of Al were machined into small strings using mechanical cutting machine and finally made into small pieces using scissors and crushed to powder with the help of a mortar and a pestle. Mechanical milling of the crushed powders was carried out using high energy planetary ball mill.

2.2 Arc melting furnace

The intermetallic alloy samples were prepared under an inert argon gas atmosphere in arc melting furnace. Arc melting is a simple but effective method in which electric arc is used to melt the constituent elements for making an alloy. The arc melting furnace consists of mainly two parts (i) a hearth with cups of one electrical polarity and (ii) electrodes with opposite polarity. Elements to be melted are placed in a cup of the hearth and the electrodes are used to strike the arc for melting the materials. Temperatures in excess of 3000^{o}C can be attained in such a furnace.

Pure constituents of the material to be melted are placed in the cup of the hearth. Small piece of titanium is also placed in a small, separate cup of the hearth. The hearth is inserted into the tapered hole in the bottom of the furnace and clamped into position. The furnace is then purged by a mechanical pump, followed by backfilling with inert argon gas. A suitable current is then set in the power supply. Initially, a piece of titanium is melted by striking arc to remove any possible oxygen impurity from the

argon gas. Then the arc is struck on the material to be melted under the continuous flow and homogenous melt. The specimen is turned over and remelted several times to ensure the homogeneity of the sample. Then the arc is turned off by gradually decreasing the current from the power supply.

2.3 High energy ball milling

High energy ball milling experiments starting from elemental powder mixtures or from pre-alloyed materials was performed using high energy planetary ball mill. The

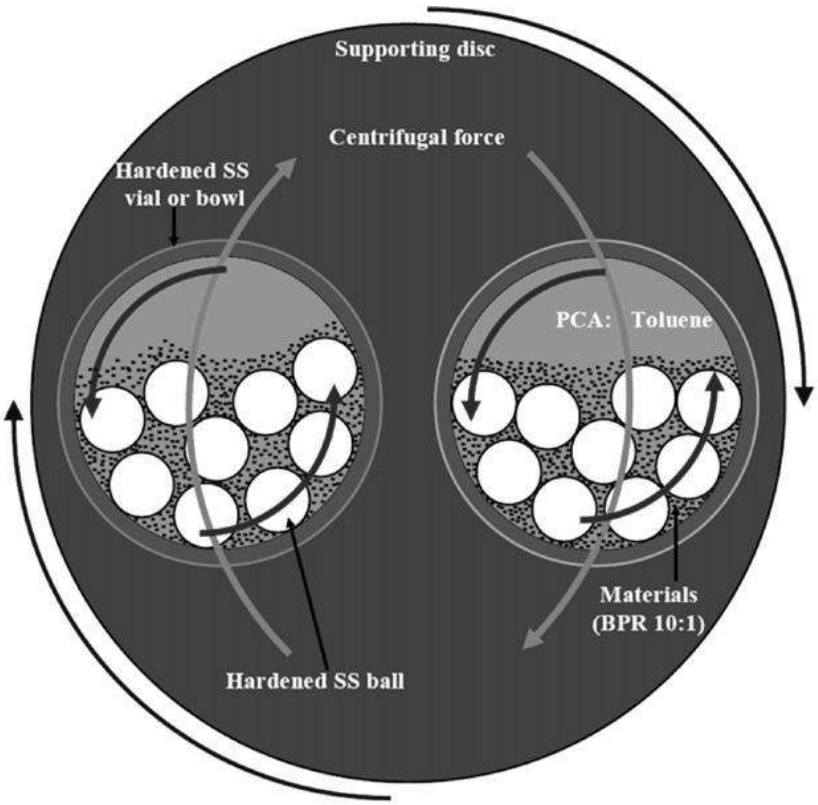

Figure 2.1: Schematic of depicting the ball motion inside the two station high-energy ball mill [Sivasankaran *et al*. (2010)].

planetary ball mill owes its name to the planet-like movement of its vial (s). Since the vials and the supporting disc rotate in opposite directions, the centrifugal forces

alternatively act in like and opposite directions. This causes the milling balls to run down the inside wall of the vial- the friction effect, followed by the materials being milled and milling balls lifting by of and travelling through the inner chamber of the vial and colliding against the opposite inside wall [Suryanarayana (2001)]. Planetary mills exploit the principle of centrifugal acceleration instead of gravitational acceleration. The enhancement of the forces acting on the ball in relation to the conventional ball mill is achieved by the combined action of two centrifugal fields [Golosov (1971) and Molcanov *et al*. (1988)]. The charge inside vials performs two relative motions: a rotary motion around the mill axis and a planetary motion around the vial axis (Fig. 2.1). The schematic illustration of synthesis of materials using planetary ball mill is shown in Fig. 2.1.

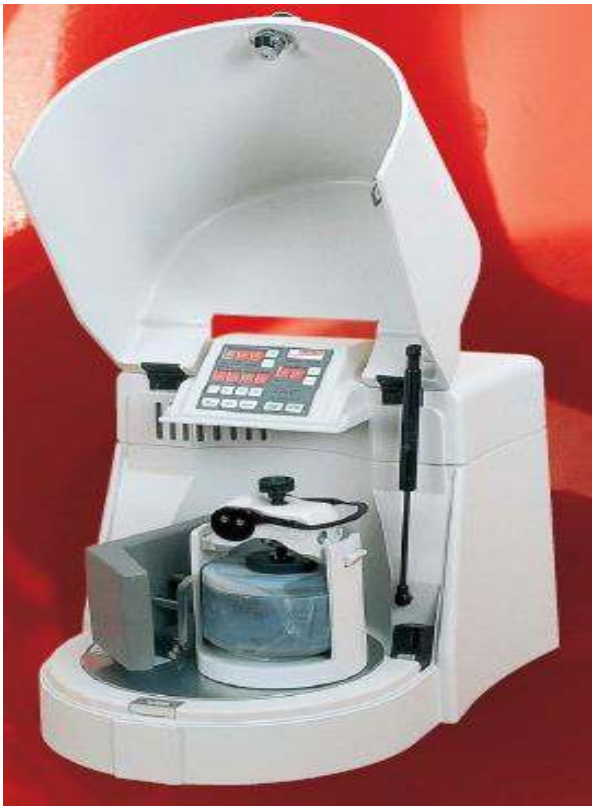

Figure 2.2: Fritsch P-6 pulverisette planetary ball mill set up.

High-energy ball milling of matrix powders and reinforcements for Al-based composites and Al-Fe intermetallics was carried out in a Fritsch P-6 Pulverisette (Fig. 2.2), for different periods of time raging from 0 to 50 h at 300 rpm with a ball to powder weight ratio (BPR) of 10:1. The vials and balls were made of hardened stainless steel. Initially the vials were evacuated and then the starting materials for the milling experiments along with toluene were charged into the vial. The milling operation was performed under toluene, a process control agent, to prevent the formation of oxides during milling and to minimize the extreme tendency of powders to get welded during milling. To avoid over-heating during milling, experiments were paused for 5 min periodically after every 20 min of milling. The milling operation was intermittently stopped after milling durations of 10, 20, 30, 40 and 50 h for the purpose of monitoring the effect of ball milling.

2.4 Characterization techniques

The characterization of the as-cast alloys and MA/MA powder samples was done using various techniques. The identity of phases, crystallite size and sequence of phase evolution at different stages of mechanical milling were studied by X-ray diffraction analysis (XRD). Differential thermal analysis (DTA) was conducted to study the thermal stability of the as-cast and milled samples. Particle size distribution was determined using a laser diffraction particle size analyzer. The microstructure was analyzed by Scanning, transmission and high resolution transmission electron microscopy. Microhardness and nanohardness of the samples were carried out using Vickers microhardness and nanoindentation to study the mechanical behavior. The above techniques employed are discussed briefly in the present chapter.

2.4.1 Chemical analysis

Chemical composition of the ingots obtained was confirmed using atomic absorption spectrophotometer (AAS). Elemental analyses of the samples by energy dispersive X-ray spectroscopy were performed on a JEOL 840A scanning electron microscope. Typical data collections utilize a 20 kV accelerating voltage and a 30 mA beam current.

2.4.2 Particle size analysis

The particle size distribution of the nano-composite powders milled for 50 hour was determined using a laser diffraction particle size analyzer (Master sizer, Malvern, U.K). A laser diffraction particle size analyzer measures size distribution of particles by applying the principles of light scattering. Laser diffraction technique provide more reliable PSD measurements on account of ease of use and broad size ranges, from nanometers to millimeters [Xu *et al*. (2003)].

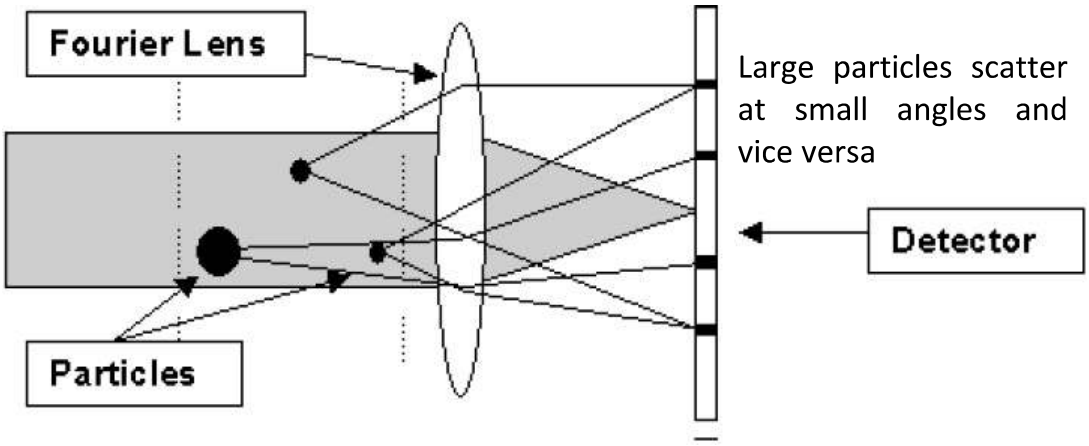

Figure 2.3: Fourier optics [Beckman Coulter (2003)].

The laser diffraction technique relies upon the fact that particles will act as scattering centers when exposed to beam of light; thus resultant patterns of scattered light can be produced and analyzed mathematically, with the assumption of spherical particles. Based on the Mie Theory, the scattering pattern of particles is directly related to particle size. As shown in Fig. 2.3, larger particles scatter at smaller angles while smaller particles scatter at larger angles. Particle-size analysis data can be presented and used in several ways, the most common being a cumulative particle-size distribution curve. The percentage of particles less than a given particle size is plotted against the logarithm of the effective particle diameter. Particle-size distribution curves, when differentiated graphically, produce frequency distribution curves for various particle sizes. Frequency curves usually exhibit a peak or peaks representing the most prevalent particle sizes.

D_{50} and D_{90}-D_{10} values indicative of the average particle diameter equivalent to 50 % of the particles undersize this value and spread of particle size distribution was estimated from PSD curve. Sample for particle size analysis was prepared by dispersing a small amount of powder in deionized water with constant ultrasonic vibration and magnetic stirring for 30 minutes each. Then the sample was kept in a sample holder with the help of syringe for analysis.

2.4.3 X-ray diffraction

X-ray powder diffraction (XRD) is an analytical technique primarily used for phase identification of a crystalline material and can provide information on unit cell dimensions. This technique is based on constructive interference of monochromatic X-rays and a crystalline sample. These X-rays are generated by a cathode ray tube, filtered to produce monochromatic radiation, collimated to concentrate, and directed toward the sample. The interaction of the incident rays with the sample produces constructive

interference (and a diffracted ray) when conditions satisfy Bragg's law ($n\lambda=2d\sin\theta$). This law relates the wavelength of electromagnetic radiation to the diffraction angle and the lattice spacing in a crystalline sample. These diffracted X-rays are then detected, processed and counted. By scanning the sample through a range of 2θ angles, all possible diffraction directions of the lattice should are obtained due to the random orientation of the powdered material. The structural evolution of composite powders and intermetallics during milling was performed using an automated D8 Discover Bruker diffractometer with CuK_{α} radiation (λ = 0.15406 nm) operated at 40kV/30mA. Scanning was performed form 20^0 to 90^0 at 0.01 degree steps and at the rate of 2^o/min. These conditions were maintained intact throughout the entire course of the experiment. The qualitative phase analysis was performed by the usual Hanawanlt's method of comparative peak matching with the standard JCPDS files. The "d" spacing is calculated for different samples from the diffraction data obtained using Bragg's law. The "d" values are matched with those existing in JCPDS files for the identification of different phases.

The average crystallite size and lattice micro-strain of the milled powders were determined from the Full-Width at Half Maximum (FWHM) of diffraction peaks, using Williamson and Hall method [Williamson *et al*. (1953)] after removing the instrumental broadening. The significance of broadening of the Bragg peak has been evidenced to crystallite size refinement along with large strain associated with powder and instrumental broadening. Full width at half maximum (FWHM) of the Bragg peaks as a function of diffraction angle was analyzed. As peak broadening will be due to grain size refinement, strain induced and instrument broadening. Before calculating the crystallite size and strain induced in the specimen, instrumental broadening was subtracted by

calibration with standard silicon sample. The X-ray peak broadening due to small crystallite size is inversely proportional to $\cos\theta$, and directly proportional to $\tan\theta$ due to lattice strain. By combining these two effects one can get equation (after subtraction of the instrumental broadening) as:

$$\beta = 0.9\frac{\lambda}{t\cos\theta} + \varepsilon\tan\theta \quad (2.1)$$

Where, t is the crystallite size, λ is the wavelength of the X-ray radiation used, β is the peak width at half the maximum intensity, θ is Bragg angle and ε is the strain. After rearrangement, the above equation can be written as:

$$\beta\cos\theta = 0.9\frac{\lambda}{t} + \varepsilon\, sin\,\theta \quad (2.2)$$

Thus, when $\beta\cos\theta$ is plotted against $\sin\theta$, a straight line (Williamson - Hall plot) is obtained with slope as ε and intercept as $0.9\,\lambda/t$. From, these one can calculate the crystallite size and lattice strain [Klug *et al.* (1967) and Cullity (1978)].

For intermetallics the average crystallite size and micro-strain of the as-cast ingots and ball milled powders were measured by Voigt function of single line approximation method [De Keijser *et al*. (1982)]. For samples with very high crystallite content the peaks were well separated and could be fit individually very successfully with Voigt method profile fitting. The samples with higher amorphous fractions could not be adequately analyzed with this technique due to heavy overlap between the very broad crystal peaks and the two amorphous peaks. In order to decompose these peaks a sophisticated peak fitting routine known as the Reitveld method was used. In Reitveld method, instead of merely fitting the peaks shapes individually the optimization routine manipulates the parameters of the model to fit all the peaks from that phase together.

2.4.4 Scanning electron microscopy

Scanning electron microscopy (SEM) is a powerful technique for microstructural analysis. This is a type of electron microscope that produces images of a sample by scanning over it with a high energy focused beam of electrons. The electrons interact with electrons in the sample, producing secondary electron, back-scattered electrons, and characteristic X-rays that can be detected and that contain information about the samples surface topography and composition. Schematic illustration of SEM is shown in Fig. 2.4. The electron beam is generally scanned in a raster scan pattern, and the beam's position is combined with the detected signal to produce an image. The electron beam obtained can be focused to a spot approximately 1 nanometer in diameter, and microscopes are able to resolve details ranging from 1-20 nm in size.

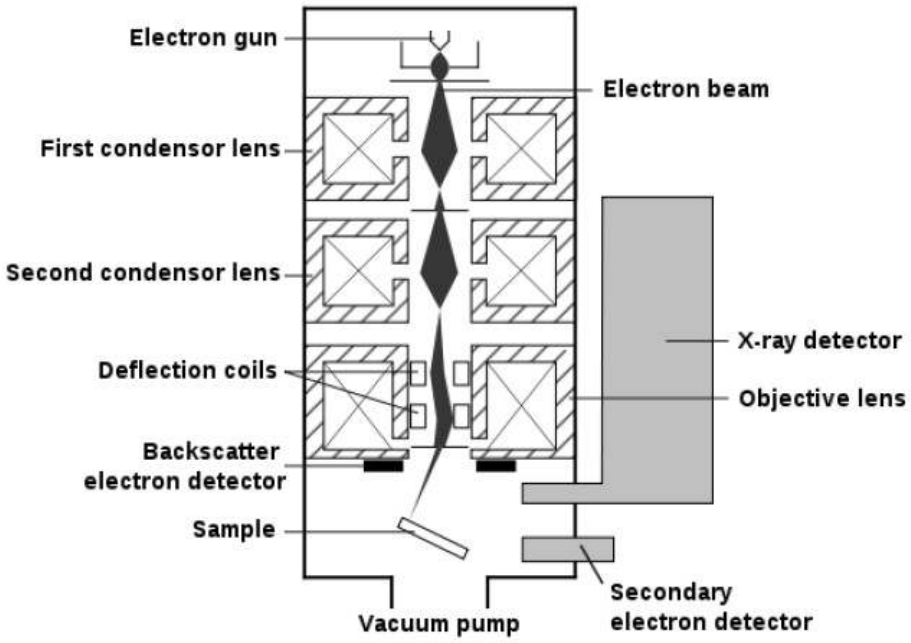

Figure 2.4: Schematic diagram of scanning electron microscopy [Goldstein *et al.* (2003)].

The type of signals produced by a SEM includes secondary electrons (SE), back-scattered electrons (BSE), characteristic X-rays, light cathodoluminescence (CL), specimen current and transmitted electrons. In general, SEM images can be obtained using SE and BSE. SE image provides topographical information and back scattered electrons can be used to detect contrast between areas with chemical compositions. This technique provides a large depth of field, which means, the area of the sample that can be viewed in focus at the same time is quite large [Flegler *et al*. (1993)]. SEM can be equipped with an energy dispersive X-ray spectrometer (EDAX) or a wavelength dispersive X-ray spectrometer (WDS). The chemical composition and mapping can be inferred using EDAX system. In this work, the external morphology of as received and ball milled powders was examined using JEOL, 840A scanning electron microscope (SEM) operated at 15 kV. Samples were prepared by sprinkling the loose powder on an adhesive stub and then examined using secondary electron imaging mode.

2.4.5 Transmission electron microscopy

Transmission Electron Microscope (TEM) is based on the theory where energetic electrons are imposed on the surface of the experimental nanoparticles to evaluate the morphologic, compositional and crystallographic information of the particle. TEM is the most powerful magnified microscope capable of evaluating particles even less than 1 nm. Transmission electron microscopy (TEM) involves a high voltage electron beam emitted by a cathode and formed by magnetic lenses. The electron beam that been partially transmitted through the very thin specimen carriers information about the structure of the specimen. The spatial variation from the obtained

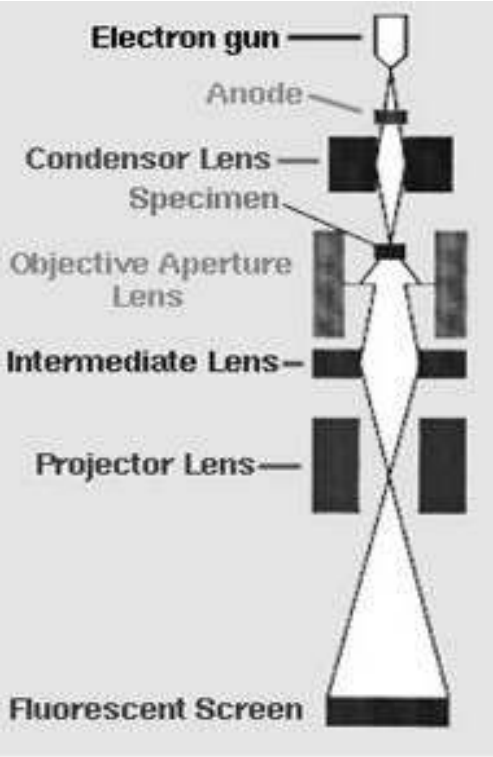

Figure 2.5: Schematic diagram of transmission electron microscopy [Williams *et al.* 1996].

image is then magnified by a series of magnetic lenses until it is recorded by a hitting fluorescent screen, photographic plate, or light sensitive sensor such as charge coupled device camera. Schematic diagram of the transmission electron microscope is shown in Fig. 2.5. Microstructural analysis and further confirmation of XRD analysis was carried out by means of FEI Tecnai-20 G^2 transmission electron microscope operated at 200 kV. For TEM sample preparation, the powder samples were dispersed ultrasonically in acetone and a liquid drop with dispersed particles was dried on a carbon coated Cu gird. Bright field and dark field images of the powder were taken at different magnifications.

Selected area electron diffraction (SAD) patterns of the same were taken by fixing the working length of TEM at 155 mm.

2.4.6 High resolution transmission electron microscopy

HRTEM provides structural information at atomic resolution ~ 0.1 nm. The position of the individual atomic columns in a crystalline sample can be well resolved in specific orientations of the crystals. Interpreting an HRTEM image is not always straightforward, and if quantification is needed, image simulation is required to match proposed structures to image contrast. Though the contrast in HRTEM image is reduced, crystalline features can be resolved. HRTEM in this study was used to qualitatively distinguish between crystalline and amorphous phases obtained in single as-milled nanoparticles. The HRTEM images in this work were recorded by using JEOL JEM 2200FS transmission electron microscope operated at 200 kV.

2.4.7 Differential thermal analysis

The thermal behavior of milled powders was examined to study the phase decomposition/dissolution reactions, if any, using INS SDT-Q600 differential thermal analyzer (DTA). This technique involves heating or cooling a test sample and an inert reference under identical conditions, while recording the temperature difference between the sample and reference. The differential temperature is then plotted against time, or against temperature (DTA curve or thermogram). Changes in the sample lead to the absorption (endothermic event) or evolution of heat (exothermic event) relative to the inert reference. Differential temperatures can also arise between two inert samples when their response to the applied heat treatment is not identical. Hence DTA can be used to study phase changes and thermal properties which do not necessarily lead to a

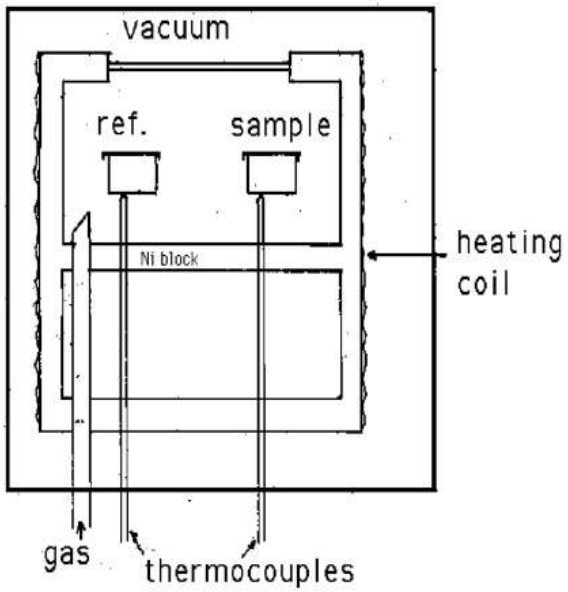

Figure 2.6: Schematic illustration of a DTA instrument.

change in enthalpy. The baseline of the DTA curve exhibits discontinuities at transition temperatures and the slope of the curve at any point will depend on the microstructural constitution at that temperature. Schematic illustration involving key features of DTA instrument are shown in Fig. 2.6. In this work to prevent oxidation and to control the operating pressure during analysis circulation of inert gas was employed. About 10-20 mg of as-milled powder material was charged with a heating rate of 20^{o}C/min and 10^{o}C/min for Al-based composites and intermetallics respectively.

2.5 Mechanical testing

2.5.1 Microhardness analysis

Microhardness measurements of the individual powder particles were carried out using standard Vickers microhardness tester (UHL-VMHT, LEICA). Vickers hardness

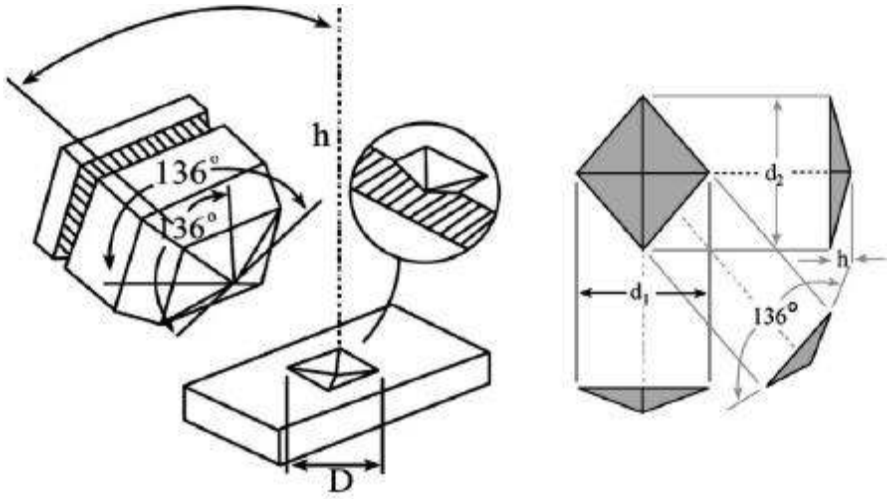

Figure 2.7: Schematic diagram of the Vickers indenter and an indentation diagonal length [Guder *et al.* (2011)].

test uses diamond indenter in the form of square-based pyramid for which the angle between the two opposite sides is equal to 136° (Fig. 2.7). The representative area corresponds to the true area of the contact between the pyramid and the material at the maximum load of the indentation. By means of simple geometrical considerations, the contact area may be expressed as a function of the diagonal of the indent. The Vickers microhardness (H_V) is calculated using the formula as given in equation 2.3

$$H_V = \frac{P}{A_V} = \frac{P}{\left(\frac{d^2}{2}\right)\sin\left(\frac{\theta}{2}\right)} = 1.8544\frac{P}{d^2} \qquad (2.3)$$

Where P is the applied test load in N, d is the average of two indentation diagonal lengths in μm, θ (=136°) is the angle between the opposite faces of the diamond pyramid indenter and 1.8544 is a geometrical constant of the diamond pyramid. A load

of 10 g with dwell time of 10 s and a load of 25 g with dwell time of 20 s was employed for Al-based composite and intermetallic powders respectively. The reported hardness values are an average of at least 5 to 8 measurements. The specimens for hardness measurements were prepared by mixing a small quantity of milled powder with the mounting material Epoxicure (supplied by Buehler). The cured mounts were then successively polished to obtain using standard metallographic technique. The final polishing was accomplished by 0.05 μm alumina powder suspension for composite powders and paste containing diamond particles with a diameter smaller than 0.25 μm for intermetallic powders. The mounting material used was hard enough to support the particles under the applied load. The indentation sites on these samples were chosen to be within the grain interior and away from grain boundaries and microscopic pores.

2.5.2 Nanoindentation

The hardness and modulus of elasticity of the milled powders were evaluated using a MTS Nano Indentor XP employing the Oliver and Phar technique [Oliver *et al*. (2004)]. Hardness testing was done with a Berkovitch tip under a load control of 100 mN and 20 mN per minute for nano composite and intermetallic powders respectively. To obtain statistical significance on the hardness and elastic modulus about 1-8 indentations tests were performed on one particle depending on the size. The schematic representation of loading versus displacement during nanoindentation is shown (Fig. 2.8).

Fig. 2.9 shows a typical plot of load P versus depth of indentation h for a sharp indenter. In the figure, S represents the contact stiffness while h_c is the contact depth, h_f is the depth of the residual impression and h_{max} the maximum indentation depth on loading. The loading part of the curve is assumed to contain both plastic and elastic

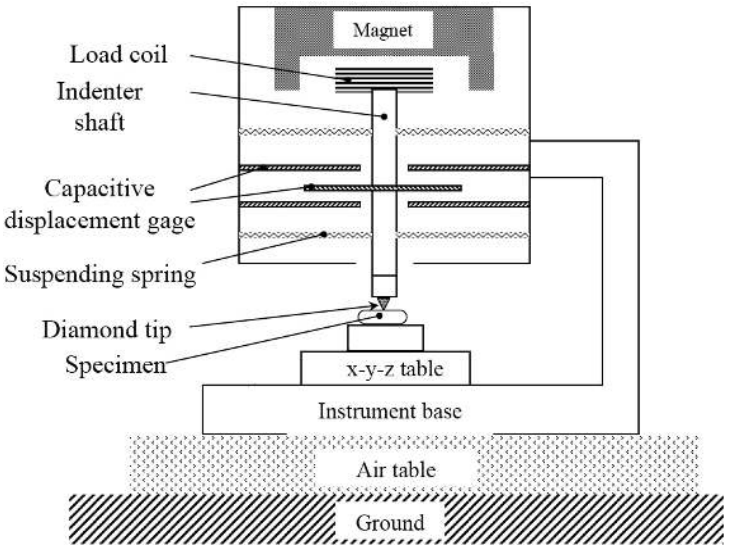

Figure 2.8: A schematic diagram of a nanoindenter that uses a load coil to impose the load and capacitive gages to measure the displacement [Wright *et al.* (2013)].

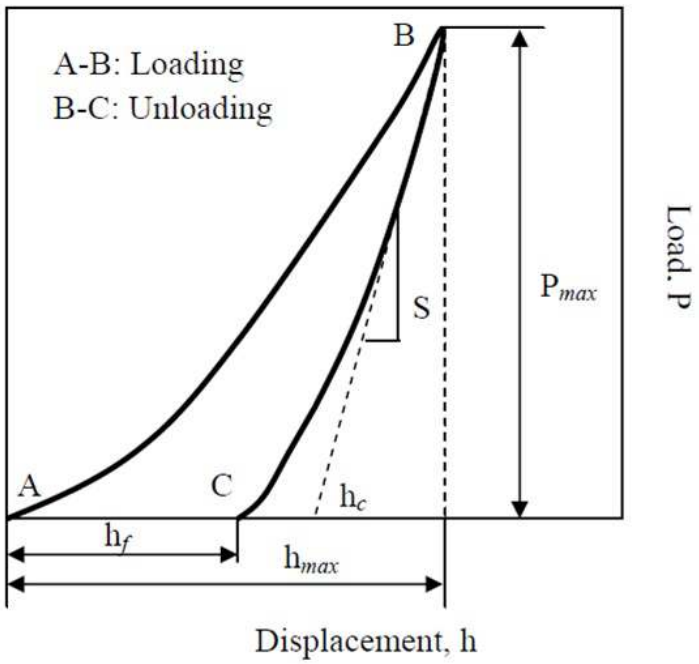

Figure 2.9: Typical load P as a function of depth h for indentation with a sharp indenter illustrating the depth of the residual hardness impression h_f, the maximum indentation depth h_{max}, and the unloading stiffness S [Xia *et al*. (1998)].

deformation, while the unloading portion of the curve is assumed to be purely elastic. In addition to this curve, the indenter tip used is carefully characterized by generating an area function, which is just the cross sectional area of the tip in contact with a sample at a given depth. The contact area of the indentation is then simply the value of the area function at the contact depth. The hardness is calculated according to

$$H = \frac{P_{max}}{A_c} \tag{2.4}$$

where P_{max} is the maximum indentation load and A_c is the projected contact area under load between the indenter and the material being indented. The procedure adopted for the specimen preparation for nanoindentation experiments were same as specified in section 2.5.1.